

See discussions, stats, and author profiles for this publication at: <https://www.researchgate.net/publication/264637176>

Photodegradation of Pyrene on Al₂O₃ Surfaces: A Detailed Kinetic and Product Study

ARTICLE in THE JOURNAL OF PHYSICAL CHEMISTRY A · AUGUST 2014

Impact Factor: 2.69 · DOI: 10.1021/jp504725z · Source: PubMed

CITATION

1

READS

37

7 AUTHORS, INCLUDING:



Manolis N Romanias

Ecole des Mines de Douai

25 PUBLICATIONS 99 CITATIONS

SEE PROFILE



Aurea Andrade-Eiroa

French National Centre for Scientific Research

27 PUBLICATIONS 231 CITATIONS

SEE PROFILE



Roya Shahla

CNRS Orleans Campus

5 PUBLICATIONS 8 CITATIONS

SEE PROFILE



Yuri Bedjanian

CNRS Orleans Campus

67 PUBLICATIONS 853 CITATIONS

SEE PROFILE

Photodegradation of Pyrene on Al_2O_3 Surfaces: A Detailed Kinetic and Product Study

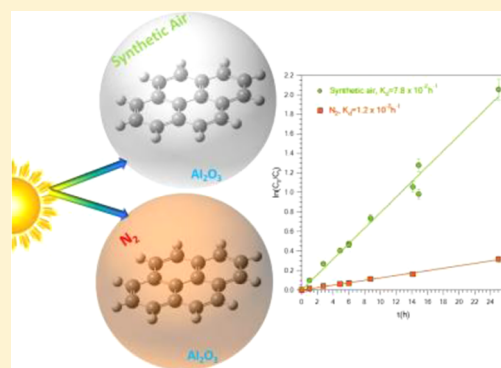
Manolis N. Romanias,^{*,†} Auréa Andrade-Eiroa,[†] Roya Shahla,[†] Yuri Bedjanian,[†] Antonia G. Zogka,[†] Aggelos Philippidis,[‡] and Philippe Dagaut^{*,†}

[†]Institut de Combustion, Aérothermique, Réactivité et Environnement (ICARE), CNRS-INSIS, 1C, Avenue de la Recherche Scientifique, 45071 Orléans Cedex 2, France

[‡]Institute of Electronic Structure and Laser, Foundation for Research and Technology-Hellas (IESL-FORTH), P.O. Box 1385, GR 711 10 Heraklion, Crete, Greece

S Supporting Information

ABSTRACT: In the current study, the photochemistry of pyrene on solid Al_2O_3 surface was studied under simulated atmospheric conditions (pressure, 1 atm; temperature, 293 K; photon flux, $J_{\text{NO}_2} = 0.002\text{--}0.012\text{ s}^{-1}$). Experiments were performed using synthetic air or N_2 as bath gas to evaluate the impact of O_2 to the reaction system. The rate of pyrene photodegradation followed first order kinetics and was enhanced in the presence of O_2 , $k_d(\text{synthetic air}) = 7.8 \pm 0.78 \times 10^{-2}\text{ h}^{-1}$ and $k_d(\text{N}_2) = 1.2 \pm 0.12 \times 10^{-2}\text{ h}^{-1}$ respectively, due to the formation of the highly reactive $\text{O}_2^{\bullet-}$ and HO^{\bullet} radical species. In addition, k_d was found to increase linearly with photon flux. A detailed product study was realized and for the first time the gas/solid phase products of pyrene oxidation were identified using off-line GC-MS and HPLC analysis. In the gas phase, acetone, benzene, and various benzene-ring compounds were determined. In the solid phase, more than 20 photoproducts were identified and their kinetics was followed. Simulation of the concentration profiles of 1- and 2-hydroxypyrene provided an estimation of their yields, 33% and 5.8%, respectively, with respect to consumed pyrene, and their degradation rates were extracted. Finally, the mechanism of heterogeneous photodegradation of pyrene is discussed.



1. INTRODUCTION

Polycyclic aromatic hydrocarbons, PAHs, are organic contaminants widely distributed to the environment with long atmospheric lifetimes.¹ They are produced from incomplete combustion of organic materials and mainly have anthropogenic origin. They are toxic, mutagenic, and carcinogenic materials causing serious health effects to the humans.^{2,3} In the beginning of 21st century approximately 8600 and 14090 tonnes per year were emitted in United States and Europe, respectively.^{4,5}

Primary soot particles containing PAH compounds can undergo long-range transportation and finally get mixed with other aerosol particles existing in the atmosphere.^{6,7} In particular, Kim et al. have observed that mineral dust originated from North China after long-range transportation over polluted areas, was enriched with substantial concentrations of elemental and organic carbon.⁷ It has been proposed that this “mixing process” can affect the optical properties^{7,8} and hygroscopicity of the aerosol particles.⁹ Hence, they could affect the radiation balance of the planet. Moreover, the chemical reactivity of the particles can also substantially be influenced from the presence of PAHs. In our recent study,⁸ we showed that PAHs contained in soot, act as photosensitizers upon absorption of UV light promoting a sequence of redox reactions on the surface of

Al_2O_3 enhancing the photodegradation rate of NO_2 by 2 order of magnitudes, producing NO and HONO as gas phase products. Although those experiments have not been conducted with real atmospheric samples, they show that the presence of PAHs in atmospheric particles can potentially influence the NO_x and HO_x budget of the troposphere.

The decontamination of PAHs on solid surfaces has been of great interest over the past years. Regarding pyrene, there are several experimental studies concerning its photodegradation on different surfaces and the major findings are summarized in Table 1. Table 1 also reveals the wide discrepancy between the results obtained from different groups studying the same reaction system; for example, degradation rate differs by ~ 10 times for fly ash. Although in the majority of the published data various products have been reported,^{10–12} a detail product study including quantification of the product yields and analyzing simultaneously the gas and solid phase has never been realized until now. Therefore, complementary studies of particulate PAH photodegradation, providing kinetic/product data are necessary to establish the reaction mechanism and to

Received: May 13, 2014

Revised: July 30, 2014

Published: August 7, 2014

Table 1. Summary of Literature Data for Pyrene Photodegradation

substrates	k_d (10^{-2} h^{-1})	light source	refs
soil	1.51	$\lambda = 253.7 \text{ nm}$ $k_d \approx \Phi^{1/2}$ ($1.19\text{--}3.57 \text{ W/m}^2$)	13, 14
soil/TiO ₂			
soil	0.11	$\lambda = 254 \text{ nm}$ (10.71 W/m^2)	15
fly ash	0.3	simulated sunlight	16
	1.51	$\lambda = 300\text{--}400 \text{ nm}$ (17.6 W/m^2)	17
	2.95 ± 1.63	dark	18
	10.30 ± 3.51	$\lambda = 300\text{--}400 \text{ nm}$ (36 W/m^2)	
black carbon	0.07	$\lambda = 300\text{--}400 \text{ nm}$ (17.6 W/m^2)	17
α -FeOOH	23.01	$\lambda_{\text{max}} = 365 \text{ nm}$ k_d independent of Φ ($4.1\text{--}48 \text{ W/m}^2$)	11
γ -FeOOH	18.64		
α -Fe ₂ O ₃	20.84		
γ -Fe ₂ O ₃	18.29		
snow	100.8 ± 10.8	simulated sunlight	19
Al ₂ O ₃	2.24	$\lambda = 300\text{--}400 \text{ nm}$ (17.6 W/m^2)	17
γ -Al ₂ O ₃	7.8 ± 0.78 (synthetic air)	$\lambda = 315\text{--}400 \text{ nm}$ $k_d \approx \Phi$ $J_{\text{NO}_2} = (2\text{--}12) \times 10^{-3} \text{ s}^{-1}$	this work
	1.2 ± 0.12 (N ₂)		

better assess the potential health risk of PAHs and their impact on the atmosphere.

To this end, in the current study, we report the photodegradation rate coefficient of pyrene on Al₂O₃ surfaces under relevant atmospheric conditions (pressure, P , temperature, T , and photon flux, Φ). γ -Al₂O₃ was used as model compound to mimic the mineral aerosol since it is the second most abundant component (after SiO₂) of mineral dust which represents the largest mass emission rate of aerosol particles at a global scale.²⁰ Similarly, pyrene was used as reference PAHs compound since it is one of the most abundant PAHs that exist in the atmosphere mostly in the particulate phase because of its low vapor pressure. Experiments were performed using synthetic air or pure N₂ to evaluate the impact of O₂ to pyrene and in general to PAHs degradation, an issue that has never been evaluated until now. The dependence of k_d on irradiance intensity was also determined providing significant information regarding the initial steps of the photocatalytic processes on the mineral surface. Finally a detailed product study was realized and for the first time the gas/solid phase products of pyrene oxidation were identified using off-line GC-MS and HPLC analysis and the corresponding mechanistic scheme is proposed. The ultimate goal of this article is to elucidate the mechanism of PAHs photodegradation on mineral aerosol surfaces, designate the major pathways of the degradation mechanism via the determination (qualitative and quantitative) and the kinetic monitoring of the products formed.

2. EXPERIMENTAL SECTION

2.1. Preparation of Reactants. Solid Al₂O₃ films were deposited on the outer surface of a Pyrex tube (0.9 cm outer diameter) using γ -Al₂O₃ (Alfa Aesar) suspension in ethanol. The control of Al₂O₃ mass in the suspension allowed us to regulate the mass of coating. Subsequently, pyrene, also diluted in ethanol, was deposited dropwise on Al₂O₃ coating. The weight content of pyrene with respect to Al₂O₃ was nearly 3% (reproducibility of sample preparation was $\geq 98\%$). Finally, in order to eliminate the possible residual traces of ethanol the freshly prepared pyrene/Al₂O₃ samples were heated under pumping (0.1 Torr) for 10 min.

2.2. Measurements of Pyrene Concentrations.
2.2.1. Determination of Pyrene Initial Concentrations, $[\text{pyrene}]_0$. After the preparation of the pyrene/Al₂O₃ surface

and the heating-pumping procedure, the tube was withdrawn from the reactor and surface was mechanically removed, weighted, and diluted in 2 mL of acetonitrile. Afterward, the solution was filtered twice with PTFE filters and then analyzed by HPLC where the area of the characteristic peak of pyrene was recorded. Finally, to transform the obtained values of the integrated areas to concentrations, standards of pyrene were prepared, passed through the HPLC and the calibration factor under the current conditions was determined. In addition, it should be noted that more than 2 samples were daily tested in order to estimate the uncertainties on sample preparation, and their impact to $[\text{pyrene}]_0$.

2.2.2. Determination of Pyrene Concentrations upon Irradiation. The same procedure as described before was followed for these measurements. The only difference was that after the heating of the surface under pumping, the reactor was filled with N₂/Synthetic air and the UV lamps were switched on (for details see also section 2.3). After sufficient time of irradiation, the tube was withdrawn and the standard steps mentioned before were followed to determine $[\text{pyrene}]_t$. Finally, it should be noted that the concentrations of pyrene used are substantially higher than those observed in real samples. However, the major target of the current study is to comprehend the process of the photocatalytic removal of PAHs on minerals surfaces (mechanistic investigation) and to investigate the impact of several atmospheric relevant parameters (O₂ presence, Φ) to the degradation rate.

2.3. ASP-TSR Reactor. Pyrene photodegradation experiments were performed employing the atmospheric simulation photochemical thermostated static reactor (ASP-TSR, Figure S1 of Supporting Information). The ASP-TSR is made of a double wall Pyrex glass with total volume of 181 cm³. The temperature was regulated by circulating ethanol through the jacket of the reactor. The chamber is equipped with 4 inlets and is isolated from a high vacuum system (10^{-7} Torr) with a regulating valve. Externally, the reactor was surrounded by 6 UV lamps (Sylvania BL350, 8 W) with a broad UV emission spectrum (315–400 nm). The irradiance intensity in the reactor was characterized by direct measurements of the NO₂ photolysis frequency, J_{NO_2} , as a function of the number of lamps switched on (see light source characterization section in Supporting Information). The values of J_{NO_2} determined ranged between 0.002 and 0.012 s⁻¹, respectively, reflecting

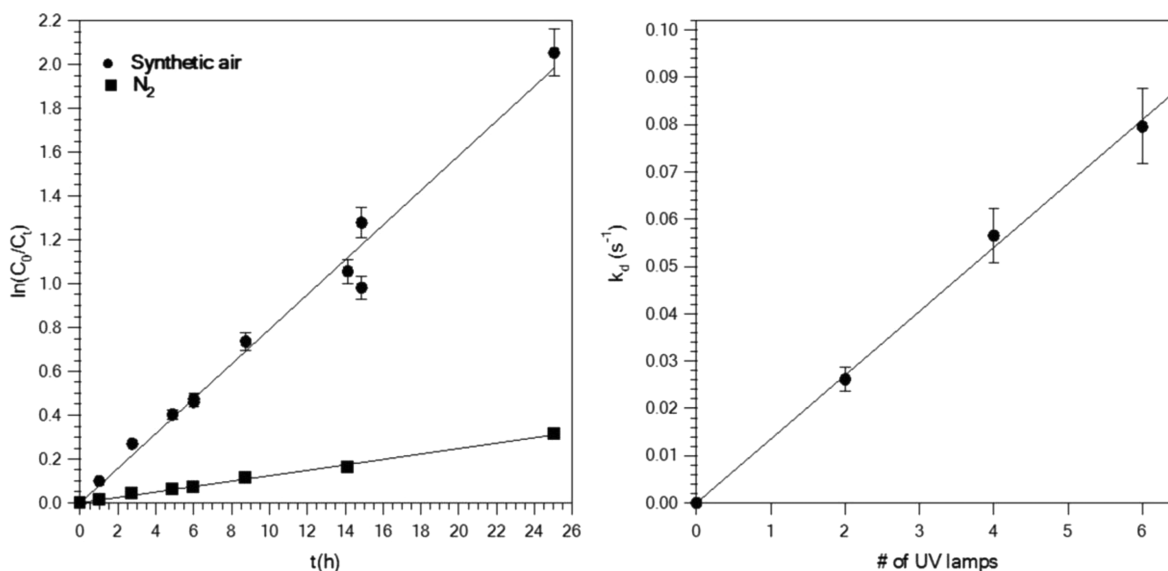


Figure 1. (a) Pyrene photodegradation kinetics on γ -Al₂O₃ surfaces under synthetic air (cycles) and pure N₂ (squares) environment and clear sky conditions ($J_{\text{NO}_2} = 0.012 \text{ s}^{-1}$). The quoted error bars reflect the 2σ precision of the fit. (b) Dependence of pyrene photodegradation rate coefficient on photon flux. The quoted error bars reflect the uncertainty in k_d measurement.

real values measured in the atmosphere under cloud and clear sky conditions.²¹ Degradation experiments were conducted at atmospheric pressure (760 Torr), using synthetic air or pure N₂ environment. At the end of each experiment, the solid surface was mechanically removed from the glass tube and diluted in 2 mL of acetonitrile for further analysis as described in section 2.2.

2.4. Gas-Phase Product Analysis. At the end of a typical photodegradation experiment, the reacted gas mixture was pumped through a Supelco thermal desorption tube, using a Teflon pump. These tubes contain multiple beds of adsorbents enabling the efficient trapping of a wide range of compounds by a single sampling. They are considered as the most common tubes used to test ambient air for toxic organic compounds. In particular, the tubes approximate analyte volatility range is n -C₃ to n -C₁₂ and the typical analytes for He Air Toxics are EPA TO-14 compounds. Subsequently the tube was driven for further elaboration employing an off-line Clarous 600c Automated Thermal Desorption GC-MS system with mass range 1–1200 amu.

2.5. Solid-Phase Product Analysis. One of the major tasks of the current study was the determination of the photodegradation products in the solid phase. The collected solid surface was analyzed using an HPLC system from Shimadzu coupled with a UV–vis photodiode array detector (PDA). Different columns and mobile phases were employed in the aim of gaining a deeper insight into the nature and structure of the pyrene photoproducts. Moreover, besides the identification of the reaction products, the kinetics of their formation was examined and the yields of 1- and 2-hydroxypyrene (products of pyrene photodegradation) were determined. The analysis of the solid surface collected was also performed with GC-MS. In this way, complementary information regarding the chemical composition of the solid surface could be obtained.

2.6. Error Analysis. In this section, we consider possible systematic contributions to the absolute uncertainty of k_d determination. They mainly include systematic uncertainties of pyrene concentration measurements (calibration experiments) and other experimental parameters, such as weight of

the masses recovered upon removal from the glass tube (<2%), volumes of the solutions prepared (<2%), reactor temperature (2%), and pressure measurement (1%). The HPLC integrated areas were measured with high precision and the 2σ was always better than 2%. The uncertainty in calibration factor of pyrene, a_M , determination was ~2%. Therefore, the estimated systematic uncertainties (accuracy) did not exceed 5%, while the overall uncertainty, including the 2σ precision of the measurements, is given by the expression $(\text{uncertainty})^2 = (2\sigma \text{ precision})^2 + (\text{systematic errors})^2$. Thus, the upper limit for k_d uncertainty was ~7%. That is why a safe upper limit of 10% to k_d measurements was given.

3. RESULTS AND DISCUSSION

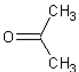
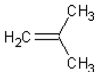
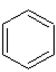
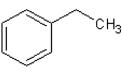
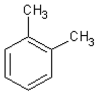
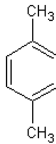
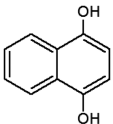
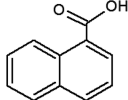
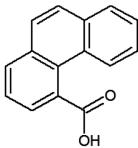
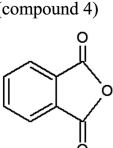
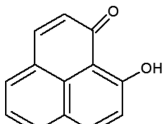
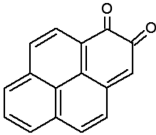
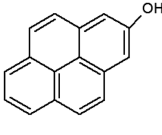
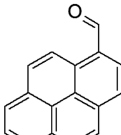
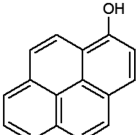
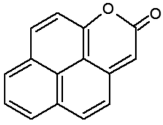
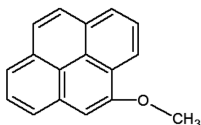
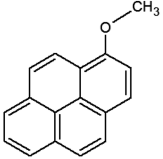
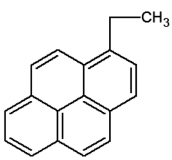
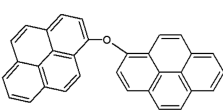
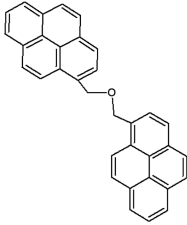
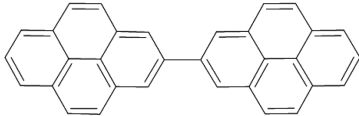
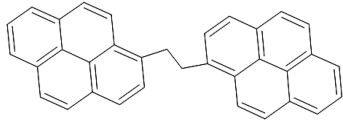

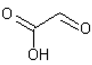
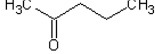
3.1. Measurement of the Photodegradation Rate.

3.1.1. Dark Reaction. The potential degradation of pyrene in the absence of light was examined in the first step of our study in order to verify that no reaction of pyrene occurs whatever the composition of the gas-phase (N₂ or synthetic air). This investigation included 3 different sets of experiments where (1) the freshly prepared Al₂O₃/pyrene surface was inserted inside the reactor heated under pumping and then directly driven for HPLC analysis to determine the absolute concentrations; (2) the surface was left for 24 hours inside the reactor under dark conditions and then driven for analysis; (3) the surface was left for 48 hours inside the reactor under dark conditions. In all cases, the absolute pyrene concentrations determined were invariant (within 5% which can be attributed to the uncertainty of our measurements) indicating that pyrene was not degraded under dark conditions inside our reactor within the time window of 48 h.

3.1.2. Degradation under UV Irradiation Conditions. The concentration of particulate pyrene followed first order exponential decay with photolysis time and the kinetics of pyrene consumption was analyzed based on the expression:

$$\ln \frac{[\text{pyrene}]_0}{[\text{pyrene}]_t} = k_d t$$

Table 2. Structures of the Identified Compounds

Gas phase products (n.r)					
Acetone 	2 methyl propene 	Benzene 	Ethyl benzene 	o-xylene 	p-xylene 
Solid phase products					
1,4-naphthalenediol (compound 1) 	1-naphtioic acid (compound 2) 	4-phenanthrene carboxylic acid (compound 3) 	1,2-benzene- dicarboxylic acid anhydride (compound 4) 	4-hydroxyperinaphthenone (compound 5) 	Isomer of compound 5
1,2-pyrene-quinone (compound 7)  a.r	2-hydroxypyrene (compound 8)  a.r	1-pyrene carboxaldehyde (compound 9) 	1-hydroxypyrene (compound 10)  a.r	2-oxapyrene-1-one (compound 11) 	4-methoxypyrene (compound 12) 
1-methoxypyrene (compound 13) 	1-ethylpyrene (compound 14) 	Unknown (compound 15)	Unknown (compound 16)	1,1'-Oxy-dipyrene (compound 17) or isomer 	Pyrene, 1,1'- (oxybis(methylene))bis- (or similar e.g 2,2'- [Oxybis(methylene)]dipyrene) 
1,1' bipyrene (compound 19) (or isomer e.g 1,4' bipyrene)  a.r or 1-[2-(1-Pyrenyl)ethyl]pyrene 	Formic acid 	Oxo-acetic acid (glyoxalic acid) 	2-butanone 		

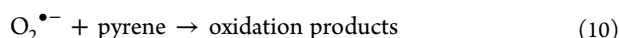
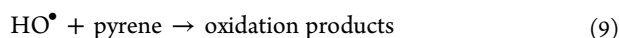
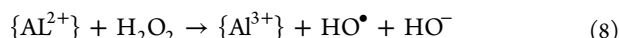
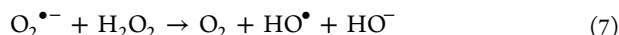
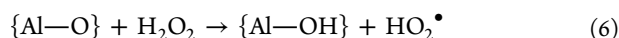
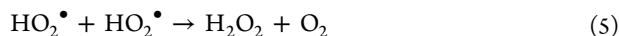
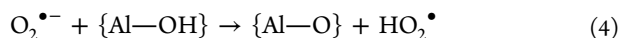
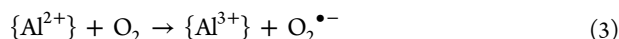
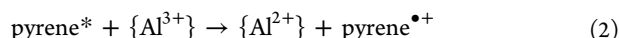
where $[\text{pyrene}]_0$ and $[\text{pyrene}]_t$ are the pyrene concentration detected with HPLC at the initial stage and after time t respectively, and k_d is the first order rate coefficient. The

obtained results are shown in Figure 1a) and Table 1. Pyrene photodegradation rate in synthetic air environment was $k_d(\text{synthetic air}) = 7.8 \times 10^{-2} \text{ h}^{-1}$, while in the presence of

N_2 was by a factor of ~ 6 lower, $k_d(N_2) = 1.2 \times 10^{-2} \text{ h}^{-1}$. This observation points that O_2 is participating to the reaction scheme, accelerating the total rate of pyrene loss. The value of k_d measured under synthetic air conditions is by a factor of 26 and 5 higher than the rates measured on fly ash and soil, respectively, and approximately 3 times lower than that on iron oxide surface (see Table 1). Although straightforward comparison of these data is problematic and not quite correct (irradiation conditions are different), they seem to indicate that k_d depends on the substrate nature. To this end, we have measured and compared the UV absorbance spectra of Al_2O_3 and SiO_2 surfaces coated with equal amount of pyrene (Figure S2 of Supporting Information material). Pyrene adsorbed on SiO_2 nanopowder appears to have higher absorption efficiency compared with pyrene coated Al_2O_3 or pure pyrene surfaces, indicating that the nature of the substrate can influence the optical properties of the adsorbed compound. Note that similar absorption spectra were recorded in the literature.^{8,22}

Al_2O_3 is not a semiconductor material. Thus, it cannot directly initiate a sequence of redox reactions, such as TiO_2 and Fe_2O_3 ; however, it may assist and enhance a photochemical process. Experimental studies have shown that γ - Al_2O_3 contains a very high density of negative charges, up to 10^{13} cm^{-2} ,²³ and also behaves as an effective hydrogen reservoir providing H atoms acting as a sponge either storing or releasing them.²⁴ EPR studies have observed that organic species initiate electron transfer reactions on the surface of alumina even under dark conditions, producing free radicals.²⁵

When a pyrene molecule absorbs the incident light an electron is promoted from the ground state to an excited one. For sake of simplicity, pyrene can be regarded as a semiconductor-like material, where the band gap corresponds to the difference between the ground and excited states (reaction 1). The lifetime of this excited state is very crucial and is limited by an electron–hole recombination process leading to emission of light or heat. Al_2O_3 seems to prevent the electron–hole recombination (reaction 2).²⁶ Subsequently, electrons are transferred to the molecular O_2 which has high electron affinity, forming a super oxide radical $O_2^{\bullet-}$ (reaction 3). $O_2^{\bullet-}$ can either react with pyrene (reaction 10) or participate in a sequence of redox reactions forming the highly reactive HO^\bullet radicals (reactions 4–8), which will initiate the oxidation of pyrene (reaction 9). This simplified mechanistic scheme supports the experimental observation of the enhanced degradation rate of pyrene in the presence of O_2 .



Note that the exact mechanism of the electron transfer from pyrene to O_2 is still unknown (reactions 1–3). It has been proposed that it takes place at the Lewis acid sites of Al_2O_3 forming a pyrene cation, $\text{pyrene}^{\bullet+}$ only in the presence of O_2 .^{10,27} Thus, reactions 3–5, proposed herein, seem to interpret the role of Al_2O_3 and O_2 as observed in our study and in the literature.

3.2. Dependence on Irradiance Intensity. The objective of the current series of experiments was to determine the photodegradation rate on Al_2O_3 surfaces as a function of the UV irradiance intensity. Experiments were performed at 293 K using synthetic air as a bath gas, and the results are presented in Figure 1b). k_d was found to increase linearly with the irradiance flux. This observation differs substantially from the data reported previously (Table 1). In particular, Dong et al.¹³ have investigated the irradiance dependence of pyrene photodegradation on soil surfaces doped with TiO_2 . From their reported data we calculated that k_d was proportional to $\Phi^{1/2}$. This trend is usually observed when the radiance flux is high and the rate of electron hole recombination becomes greater than the photocatalytic rate.²⁸ Wang et al.¹¹ have also studied the impact of irradiance intensity to the pyrene degradation rate on iron oxide surfaces. The authors found that the rate is independent of light intensity in the range of 4.1–48 W/m^2 . Unfortunately, the available data do not allow to precise the source of this (perhaps only apparent) inconsistency; it can be attributed to the nature of substrates used or to the different irradiance conditions under which the experiments were performed.

3.3. Product Analysis. **3.3.1. Gas-Phase Products Analysis.** The degradation of pyrene on Al_2O_3 surface produced various oxidation products in the gas phase (Table 2). Unfortunately, their quantification was not possible since a fraction of the gas mixture was lost (pumped) during the collection process. Acetone, benzene, ethylbenzene, *o*- and *p*-xylene, and 2 methyl propene were detected and identified by using standards of each reference compound. To our knowledge this is the first study reporting the gas phase products of particulate pyrene photodegradation.

3.3.2. Solid-Phase Product Analysis. We have used a few different approaches to analyze the solid phase. In a first one, the soluble fraction of the collected solid surface was analyzed using a phenyl column, (12.5 cm length, 4.6 mm I.D., 10 μm) using hexane as mobile phase for isocratic elution at speed flow of 0.05 mL/min and backpressure of 1 atm. Under these conditions, compounds elute strictly in order of their polarity without influence of their polarizability. The order of elution from this column is important for unambiguous characterization of some compounds (especially those showing very similar spectral features) and allows performing a preliminary study of the compound families existing in the sample. The different fractions collected using the phenyl column is presented in Figure S3 of Supporting Information material. The fraction eluted at 17.22 min contains mostly pyrene. The compounds eluted before and after pyrene appear to have lower and higher polarity, respectively.

The soluble fraction of solid surface was also analyzed using a C_{18} column (25 cm length, 4.6 mm I.D., 5 μm) under the following operating conditions: gradient elution (0–30 min, 40%–60% acetonitrile/water; 30–80 min, linear change from 40 to 100% acetonitrile; 80–100 min, 100% acetonitrile; 100–120 min, 40%–60% acetonitrile/water) at 0.5 mL/min constant flow rate. The recorded chromatogram is presented

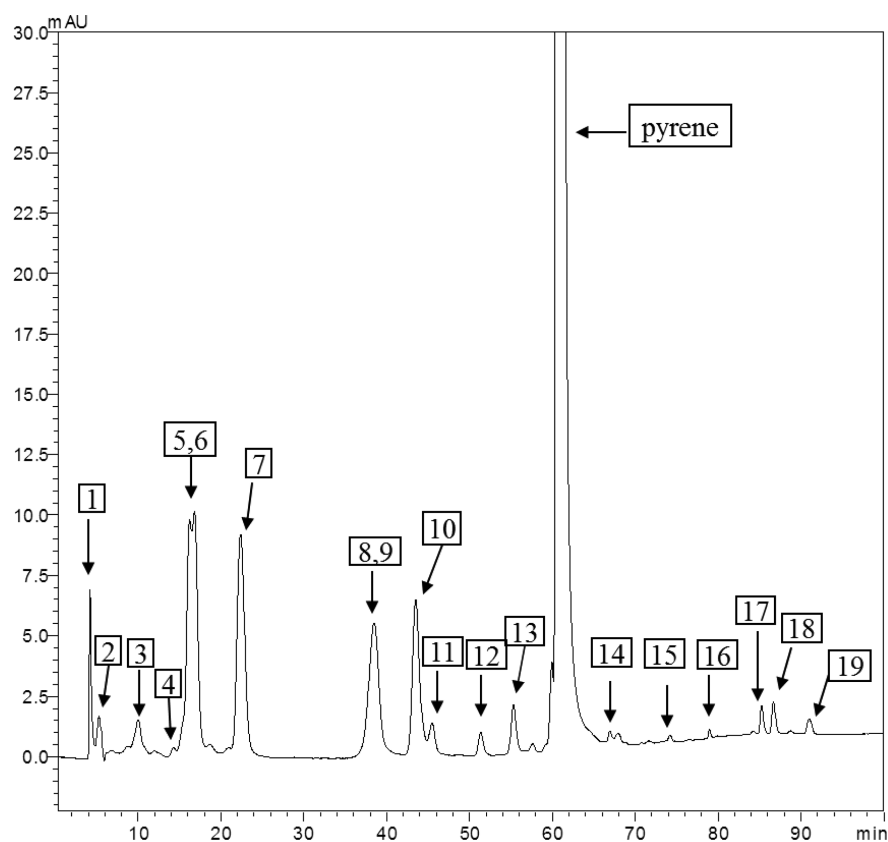


Figure 2. HPLC chromatogram recorded after 92 min of pyrene photodegradation on $\gamma\text{-Al}_2\text{O}_3$ surfaces. Elution (0–30 min, 40–60% acetonitrile/water; 30–80 min, linear change from 40% to 100% acetonitrile; 80–100 min, 100% acetonitrile; 100–120 min, 40–60% acetonitrile/water at a 0.5 mL/min constant flow rate. $T = 30^\circ\text{C}$. The chromatogram is focused in order to distinguish the pyrene photoproducts.

in Figure 2 and the different compounds eluted are numbered in the graph. As it can be seen, compounds 5, 6 and 8, 9 were not completely separated and were eluted in the same time. The chemical species 5 and 6 are isomers and their complete separation was not achieved. On the other hand, the separation of products 8 and 9 was achieved by reanalyzing the samples using 60%–40% acetonitrile/Water as mobile phase. All the compounds observed on the surface upon the photodegradation of pyrene are listed in Table 2. The collected UV spectra and detailed discussion on the identification are presented in section 4.2 of Supporting Information material.

The GC-MS analysis of the collected solid revealed even more products of the photodegradation process. Some of them, such as benzene, ethylbenzene, and *o*- and *p*-xylene, were also detected in the gas phase. The extra products observed from the GC-MS analysis of the solid surface were formic acid, 2 butanone, oxo-acetic acid (glyoxalic acid), and various C=O containing compounds that were not identified.

Only few of the compounds observed herein, or isomers of them, has already been previously reported in the literature for any kind of mineral surface. In particular, pyrenediols, pyrenediones, 1,1-bipyrene, and mono- and dihydroxypyrene are among of them.²⁹ In Table 2, the abbreviation a.r. was used to denote the “already reported” products, or their isomers, of pyrene degradation on any solid surface.

3.3.3. Kinetics of the Reaction Products. One of the major tasks of the current study was to follow the kinetics of solid-phase pyrene photoproducts. The concentrations of pyrene degradation products were monitored as a function of illumination time. The absolute concentrations of two of

them, 1- and 2-hydroxypyrene, were determined using purchased standards. Their time dependent concentration profiles and that of pyrene are presented in Figure 3. Solid lines in Figure 3 represent a simulation of the experimental data within a simplified mechanism including 1- and 2-hydroxypyrene production upon pyrene degradation and their subsequent loss. This simplified reaction scheme assumes a steady state for all the intermediate active species:

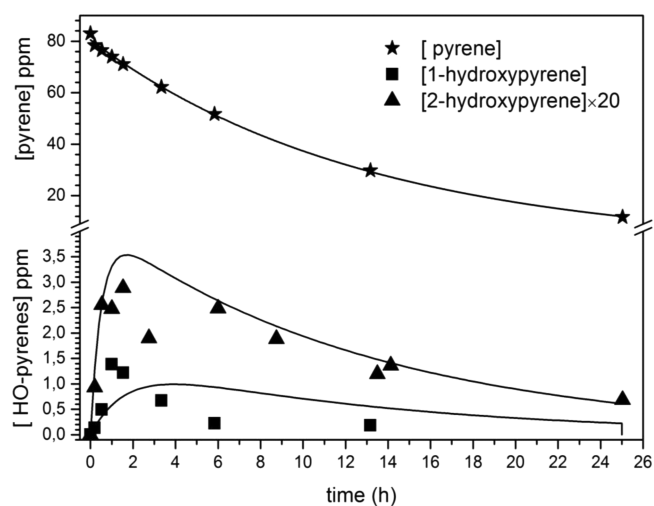
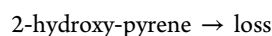
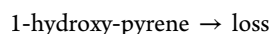
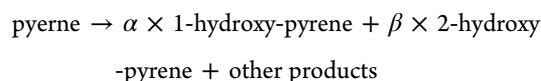


Figure 3. Time-dependent concentration profiles of pyrene, 1-hydroxypyrene, and 2-hydroxypyrene. The concentrations of 2-hydroxypyrene were multiplied for clarity purposes.



The rate of the first reaction is defined by kinetics of pyrene degradation, the yields of 1- and 2-hydroxy-pyrenes, α and β , respectively, as well as the rates of their loss were used as variable parameters and were determined from the simulation of the experimental kinetics of these species. The best fit to the experimental data was obtained with 33% (factor 2 uncertainty) and $(5.8 \pm 1.7) \%$ yields and 2 h^{-1} (factor 2 uncertainty) and $(2.3 \pm 0.7) \text{ h}^{-1}$ consumption rates for 1- and 2-hydroxy-pyrene, respectively. The observed rates of heterogeneous degradation of hydroxy-pyrenes are much higher than that of pyrene. It should be noted that the 1-hydroxypyrene data points are poorly simulated, which results in large uncertainty on the determined parameters. This may be related to the simplified reaction scheme used.

Regarding the time evolution of other reaction products, compounds 1, 2, 3, and 15 followed kinetics similar to those of 1- and 2-hydroxypyrene: we observed an initial increase of their concentrations, with a maximum reached at the same time window (after 1–1.5 h), followed by their decrease indicating consumption of these products on the irradiated surface. The concentrations were stabilized after 6 h of irradiation at relatively low levels (by a factor of ~ 5 –10 lower than the maximum values), except the unknown compound 15, which was completely consumed after 2.5 h (Figure 4). 1,2-Benzene-dicarboxylic acid anhydride, 1-methoxypyrene, and 4-methoxypyrene reached their maximum concentrations after nearly 30 min of surface irradiation. Subsequently, the concentrations of

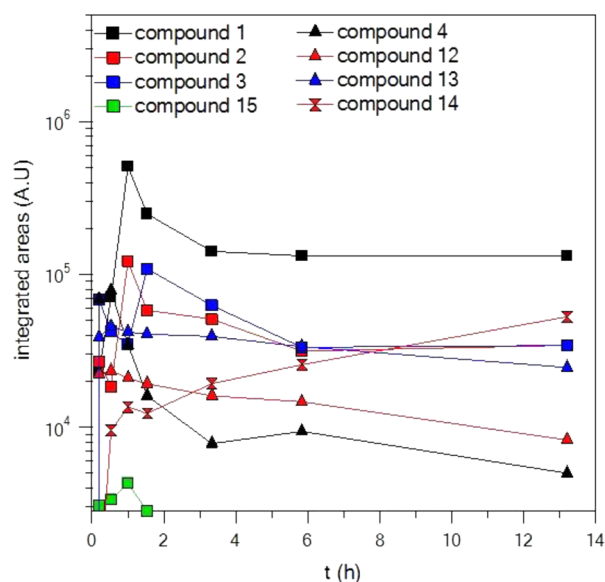


Figure 4. Time dependent profiles of several pyrene photoproducts identified. Symbols were used based on the comparison given in the text. The area for each compound was obtained upon integration of the chromatographic peak at the characteristic wavelength of absorption of each compound: compound 1 (208 nm), compound 2 (222 nm), compound 3 (216 nm), compound 4 (220 nm), compounds 12 and 13 (236 nm), compound 14 (232–242 nm), and compound 15 (237 nm).

methoxypyrenes gradually decreased with time, while 1,2-benzene carboxylic acid was almost completely consumed after 3 h (Figure 4). Conversely, the concentrations of compounds 5, 6, 7, and 11 reached their maximum after 1–1.5 h and then remained nearly invariable, at least within the first 14 h where their kinetics was recorded (Figure 5). This observation could

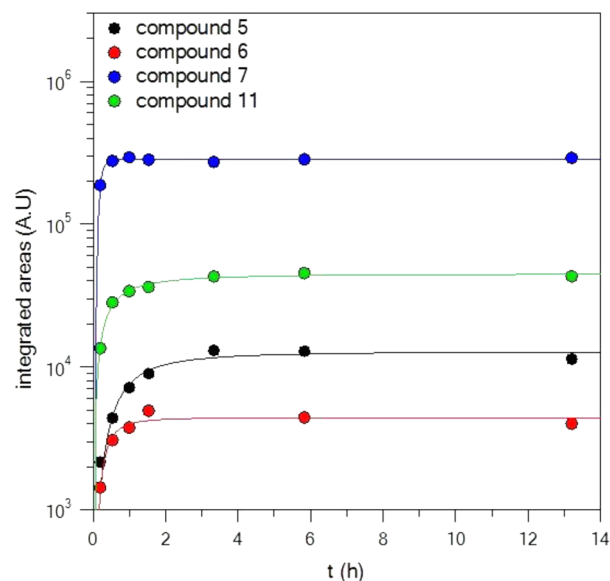


Figure 5. Time dependent production profiles of OPAHs compounds. The area for each compound was obtained upon integration of the chromatographic peak at the characteristic wavelength of absorption of each compound: compound 5 (209 nm), compound 6 (237 nm), compound 7 (238 nm), and compound 11 (234 nm). The lines were drawn just to denote the saturation regime and have no physical meaning.

be characterized as “paradox” since photodegradation of pyrene continues to take place after 1.5 h. It is difficult to explain such behavior since the concentrations of these products depends also on the concentrations of earlier oxidation products. Regarding the ethers of pyrene (compounds 17 and 18), their maximum was observed after 1–1.5 h, and the concentrations were almost stabilized at 2/3 of their maximum value after 4 h. Finally, the production of ethylpyrene was found to increase with irradiation time. The ratio of the signals of ethylpyrene production and pyrene consumption, $\Delta I_{\text{ethylpyrene}}/\Delta I_{\text{pyrene}}$ was constant indicating that the product yield was stable during the illumination process (Figure 4).

3.4. Degradation Mechanism. It is difficult to propose a step by step detailed mechanistic scheme of pyrene degradation since totally 28 different compounds have been detected as gas and solid phase products. A general reaction scheme of hydrocarbons degradation similar to those occurring in the gas phase in absence of NO_x is expected to take place.^{30,31} Thus, based on the products observed in the current study the following reaction scheme can be proposed to interpret our results. Note that the abbreviations d, nd, used in the reaction scheme denote the “determined” and “not determined” products detected.

Although the mechanism can be considered as “speculative” since only the final products and not the intermediates species were observed, similar degradation pathways have already been proposed to take place in biodegradation processes,³² and references therein. In general, pyrene degradation follows 2

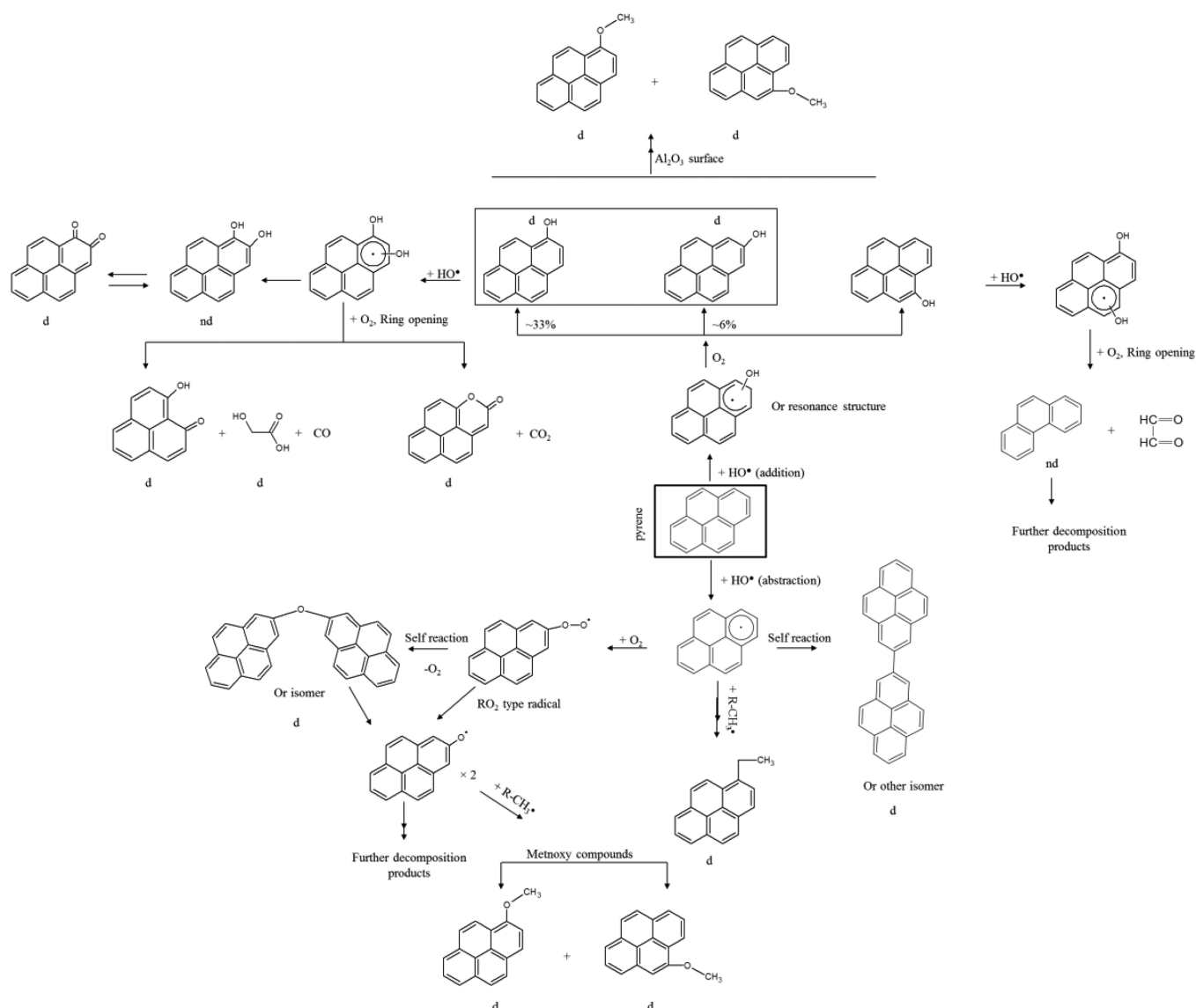


Figure 6. Proposed simple pyrene degradation mechanism.

major pathways: (a) addition of HO^\bullet radicals to the pyrene rings forming hydroxy-pyrenes or (b) H atom abstraction from HO^\bullet . The hydroxypyrenes formed after HO^\bullet addition, can be further degraded to form other oxidation products^{29,33,34} while the radicals formed via H atom abstraction can participate in self-reactions forming bipyrene, ethers of dipyrene, or further oxidation products. The formation pathways of methoxypyrenes and ethylpyrene are questionable. Methoxypyrenes can be formed after reaction of pyrene- O^\bullet type radicals (RO^\bullet) with $\text{R}-\text{CH}_3^\bullet$ radicals that have been produced from the degradation process. Another possible pathway could be their production from hydroxypyrenes as it has been observed in biodegradation processes.³² However, in biodegradation, specific enzymes catalyze this reaction which is not the case in our study. Nevertheless, literature data have shown that methoxy compounds can be formed from similar pathways on the surface of Al_2O_3 . In particular, Yamakawa et al.,³⁵ have studied the synthesis of 3-methoxy-1-propanol from methanol and allyl alcohol using metal oxides catalysts. These authors observed that methoxy-compounds formation was remarkably favorable on the surface of Al_2O_3 , and they have proposed an

analogous reaction mechanism. Thus, a plausible reaction between hydroxyl-pyrenes with degraded alcoholic compounds could be a potential source of methoxypyrenes. Finally, the mechanistic scheme proposed appears to have a gap regarding ethyl pyrene production. A possible pathway could be a sequence of reactions between methyl pyrene radicals (photolysis of compound 18 could be a possible source) with $\text{R}-\text{CH}_3^\bullet$ radicals formed from the photo-oxidation process. In addition, photolysis of 1-[2-(1-pyrenyl)ethyl]pyrene could also account to ethyl pyrene formation.

4. CONCLUSIONS

In the current study pyrene degradation rate on Al_2O_3 surface was determined under relevant atmospheric conditions using a photochemical static reactor. Experiments were performed under synthetic air or pure N_2 environment and the impact of O_2 to the kinetics and mechanism was evaluated. A rough estimation of pyrene atmospheric lifetime based on the k_d values measured under synthetic air conditions range from 76 to 13 h under cloud and clear sky conditions, respectively. For comparison, in previous study from this laboratory,³⁶ the

atmospheric lifetime of nearly 4 min was found for pyrene adsorbed on carbonaceous aerosols with respect to its oxidation by ozone under dark conditions. This seems to point that in the atmosphere, the particulate PAHs are oxidized mainly via their reactions with ozone, and, probably, with other oxidants, OH, NO₂, and NO₃. In this respect, the information on the reactivity of PAH adsorbed on mineral aerosol surface with different atmospheric oxidants and in the presence of light would be very useful.

Furthermore, for the first time, a detailed product study was conducted, including surface/gas phase analysis, and 28 different products were identified. The degradation process involves the light absorption from pyrene molecules and the transfer of an e⁻ to O₂ through the active Al₂O₃ surface sites. Subsequently, surface bound OH radicals are formed via a sequence of reactions and dominate the degradation mechanism proposed herein (Figure 6). We expect that similar photodegradation processes can take place for UV absorbing PAHs in all mineral surfaces. However, it should be noted that the proposed schemes are partially supported from our experimental results, thus a more thorough study should be realized using real atmospheric samples and employing online analytical systems in order to support and propose a coherent oxidation mechanism for PAHs on mineral surfaces.

The kinetic monitoring of 1-hydroxypyrene and 2-hydroxypyrene (1st generation products in our proposed mechanism) allowed an estimation of their yields and photodegradation rates. In addition, highly oxygenated PAHs products (OPAHs, compounds 5, 6, 7, and 11) were measured as end products of the reaction mechanism proposed. This finding seems to be of importance regarding the health risk induced by OPAHs, due to their long residence time in the atmosphere. Recently, it has been found that reactive oxygenated species are produced in larger amounts via chain reactions induced by quinone PAHs in the human body.³⁷ These compounds can cause oxidative stress connected with inflammatory diseases.³⁷ The product data from the current study provide useful information regarding the oxidation mechanism of particulate PAHs and seems to be of interest in terms of the remediation of the indoor environments and assessment of the potential health risk that may arise from the oxidized products.

■ ASSOCIATED CONTENT

■ Supporting Information

Scheme of the photochemical reactor, where the experiments were performed, details regarding the light source characterization used, solid UV spectra of Al₂O₃ and SiO₂ pure and doped with pyrene, and a detailed chapter regarding the methods followed for characterization of the solid phase products detected. This material is available free of charge via the Internet at <http://pubs.acs.org>.

■ AUTHOR INFORMATION

Corresponding Authors

*Tel.: +33 238255492. Fax: +33 238696004. E-mail: manolis.romanas@cnrs-orleans.fr.

*Tel.: +33 238255466. Fax: +33 238696004. E-mail: philippe.dagaut@cnrs-orleans.fr.

Notes

The authors declare no competing financial interest.

■ ACKNOWLEDGMENTS

The research leading to these results has received funding from the European Research Council under the European Community's Seventh Framework Programme (FP7/2007-2013)/ERC grant agreement no. 291049-2G-CSafe.

■ REFERENCES

- (1) Fernandez, P.; Grimalt, J. O. On the Global Distribution of Persistent Organic Pollutants. *Chimia* **2003**, *57*, 514–521.
- (2) Jacob, J. The Significance of Polycyclic Aromatic Hydrocarbons as Environmental Carcinogens. *Pure Appl. Chem.* **1996**, *68*, 301–308.
- (3) Henner, P.; Schiavon, M.; Morel, J. L.; Lichtfouse, E. Polycyclic Aromatic Hydrocarbon (PAH) Occurrence and Remediation Methods. *Analisis* **1997**, *25*, M56–M59.
- (4) VanJaarsveld, J. A.; VanPul, W. A. J.; DeLeeuw, F. Modelling Transport and Deposition of Persistent Organic Pollutants in the European Region. *Atmos. Environ.* **1997**, *31*, 1011–1024.
- (5) Maliszewska-Kordybach, B., Sources, Concentrations, Fate and Effects of Polycyclic Aromatic Hydrocarbons (PAHs) in the Environment. Part A: PAHs in Air. *Polym. J. Environ. Stud.*, *8*, 131–136.
- (6) Hand, V. L.; Capes, G.; Vaughan, D. J.; Formenti, P.; Haywood, J. M.; Coe, H. Evidence of Internal Mixing of African Dust and Biomass Burning Particles by Individual Particle Analysis Using Electron Beam Techniques. *J. Geophys. Res.: Atmos.* **2010**, *115*, No. D13301, DOI: 10.1029/2009JD012938.
- (7) Kim, K. W.; He, Z. S.; Kim, Y. J. Physicochemical Characteristics and Radiative Properties of Asian Dust Particles Observed at Kwangju, Korea, During the 2001 Ace-Asia Intensive Observation Period. *J. Geophys. Res.: Atmos.* **2004**, *109*, No. D19S02, DOI: 10.1029/2003JD003693.
- (8) Romanias, M. N.; Bedjanian, Y.; Zaras, A. M.; Andrade-Eiroa, A.; Shahla, R.; Dagaut, P.; Philippidis, A. Mineral Oxides Change the Atmospheric Reactivity of Soot: NO₂ Uptake under Dark and UV Irradiation Conditions. *J. Phys. Chem. A* **2013**, *117*, 12897–12911.
- (9) Miñambres, L.; Sánchez, M. a. N.; Castaño, F.; Basterretxea, F. J. Hygroscopic Properties of Internally Mixed Particles of Ammonium Sulfate and Succinic Acid Studied by Infrared Spectroscopy. *J. Phys. Chem. A* **2010**, *114*, 6124–6130.
- (10) Mao, Y.; Thomas, J. K. Photochemical Reactions of Pyrene on Surfaces Of γ -Alumina and Silica-Alumina. *Langmuir* **1992**, *8*, 2501–2508.
- (11) Wang, Y.; Liu, C. S.; Li, F. B.; Liu, C. P.; Liang, J. B. Photodegradation of Polycyclic Aromatic Hydrocarbon Pyrene by Iron Oxide in Solid Phase. *J. Hazard. Mater.* **2009**, *162*, 716–723.
- (12) Fatiadi, A. J. Effects of Temperature and of Ultraviolet Radiation on Pyrene Absorbed on Garden Soil. *Environ. Sci. Technol.* **1967**, *1*, 570–572.
- (13) Dong, D.; Li, P.; Li, X.; Xu, C.; Gong, D.; Zhang, Y.; Zhao, Q.; Li, P. Photocatalytic Degradation of Phenanthrene and Pyrene on Soil Surfaces in the Presence of Nanometer Rutile TiO₂ under UV-Irradiation. *Chem. Eng. J.* **2010**, *158*, 378–383.
- (14) Dong, D.; Li, P.; Li, X.; Zhao, Q.; Zhang, Y.; Jia, C.; Li, P. Investigation on the Photocatalytic Degradation of Pyrene on Soil Surfaces Using Nanometer Anatase TiO₂ under UV Irradiation. *J. Hazard. Mater.* **2010**, *174*, 859–863.
- (15) Zhang, L.; Xu, C.; Chen, Z.; Li, X.; Li, P. Photodegradation of Pyrene on Soil Surfaces under UV Light Irradiation. *J. Hazard. Mater.* **2010**, *173*, 168–172.
- (16) Niu, J.; Sun, P.; Schramm, K.-W. Photolysis of Polycyclic Aromatic Hydrocarbons Associated with Fly Ash Particles under Simulated Sunlight Irradiation. *J. Photochem. Photobiol., A* **2007**, *186*, 93–98.
- (17) Behymer, T. D.; Hites, R. A. Photolysis of Polycyclic Aromatic Hydrocarbons Adsorbed on Simulated Atmospheric Particulates. *Environ. Sci. Technol.* **1985**, *19*, 1004–1006.
- (18) Daisey, J. M.; Lewandowski, C. G.; Zorz, M. A Photoreactor for Investigations of the Degradation of Particle-Bound Polycyclic

Aromatic Hydrocarbons under Simulated Atmospheric Conditions. *Environ. Sci. Technol.* **1982**, *16*, 857–861.

(19) Ram, K.; Anastasio, C. Photochemistry of Phenanthrene, Pyrene, and Fluoranthene in Ice and Snow. *Atmos. Environ.* **2009**, *43*, 2252–2259.

(20) Satheesh, S. K.; Krishna Moorthy, K. Radiative Effects of Natural Aerosols: A Review. *Atmos. Environ.* **2005**, *39*, 2089–2110.

(21) Kraus, A.; Hofzumahaus, A. Field Measurements of Atmospheric Photolysis Frequencies for O₃, NO₂, HCHO, CH₃CHO, H₂O₂, and HONO by UV Spectroradiometry. *J. Atmos. Chem.* **1998**, *31*, 161–180.

(22) Boateng, B. A. S. Photophysical Properties of Pyrene, 2,7-Diazapyrene and 1,3-Bis(β -Naphthyl)propane. MS Thesis, University of North Texas, Denton, TX, 2007.

(23) Hoex, B.; Gielis, J. J. H.; van de Sanden, M. C. M.; Kessels, W. M. M. On the C–Si Surface Passivation Mechanism by the Negative-Charge-Dielectric Al₂O₃. *J. Appl. Phys.* **2008**, *104*, 113703–7.

(24) Sohlberg, K.; Pennycook, S. J.; Pantelides, S. T. Hydrogen and the Structure of the Transition Aluminas. *J. Am. Chem. Soc.* **1999**, *121*, 7493–7499.

(25) Samoilova, R. I.; Dikanov, S. A.; Fionov, A. V.; Tyryshkin, A. M.; Lunina, E. V.; Bowman, M. K. Pulsed EPR Study of Orthophosphoric and Boric Acid Modified γ -Alumina. *J. Phys. Chem.* **1996**, *100*, 17621–17629.

(26) Zhang, X.; Sutanto, I.; Taguchi, T.; Tokuhito, K.; Meng, Q.-b.; Rao, T. N.; Fujishima, A.; Watanabe, H.; Nakamori, T.; Uragami, M. Al₂O₃-Coated Nanoporous TiO₂ Electrode for Solid-State Dye-Sensitized Solar Cell. *Sol. Energy Mater. Sol. Cells* **2003**, *80*, 315–326.

(27) Dollish, F. R.; Hall, W. K. Electron Spin Resonance of 1,1-Diphenylethylene Adsorbed on Silica-Alumina Catalysts. *J. Phys. Chem.* **1965**, *69*, 4402–4405.

(28) Herrmann, J. M. Heterogeneous Photocatalysis: State of the Art and Present Applications. *Top. Catal.* **2005**, *34*, 49–65.

(29) Pagni, R.; Sigman, M., The Photochemistry of PAHs and PCBs in Water and on Solids. In *Environmental Photochemistry*; Boule, P., Ed.; Springer: Berlin, 1999; Vol. 2/2L, pp 139–179.

(30) Calvert, J. G.; Atkinson, R.; Becker, K. H.; Kamens, R. M.; Sheinfeld, J. H.; Walington, T. J.; Yarwood, G. *The Mechanisms of Atmospheric Oxidation of the Aromatic Hydrocarbons*; Oxford University Press: New York, 2002.

(31) Le Bras, G. Scientific Results. In *Chemical Processes in Atmospheric Oxidation*; Le Bras, G., Ed.; Springer: Berlin, 1997; Vol. 3, pp 13–72.

(32) Seo, J. S.; Keum, Y. S.; Li, Q. X. Bacterial Degradation of Aromatic Compounds. *Int. J. Environ. Res. Public Health* **2009**, *6*, 278–309.

(33) Zeng, K.; Hwang, H.-M.; Fu, P. P.; Yu, H. Identification of 1-Hydroxypyrene Photoproducts and Study of the Effect of Humic Substances on Its Photolysis. *Polycyclic Aromat. Compd.* **2002**, *22*, 459–467.

(34) Yu, H. T. Environmental Carcinogenic Polycyclic Aromatic Hydrocarbons: Photochemistry and Phototoxicity. *J. Environ. Sci. Health, Part C: Environ. Carcinog. Ecotoxicol. Rev.* **2002**, *20*, 149–183.

(35) Yamakawa, T.; Takizawa, M.; Ohnishi, T.; Koyama, H.; Shinoda, S. Selective Synthesis of 3-Methoxy-1-Propanol from Methanol and Allyl Alcohol with Metal Oxide Catalysts. *Catal. Commun.* **2001**, *2*, 191–194.

(36) Bedjanian, Y.; Nguyen, M. L. Kinetics of the Reactions of Soot Surface-Bound Polycyclic Aromatic Hydrocarbons with O₃. *Chemosphere* **2010**, *79*, 387–393.

(37) Chung, S. W.; Chung, H. Y.; Toriba, A.; Kameda, T.; Tang, N.; Kizu, R.; Hayakawa, K. An Environmental Quinoid Polycyclic Aromatic Hydrocarbon, Acenaphthenequinone, Modulates Cyclooxygenase-2 Expression through Reactive Oxygen Species Generation and Nuclear Factor Kappa B Activation in A549 Cells. *Toxicol. Sci.* **2007**, *95*, 348–355.